Structures and stabilities of singly charged three-electron hemibonded systems and their hydrogen-bonded isomers

ARTICLE *in* JOURNAL OF THE AMERICAN CHEMICAL SOCIETY · JULY 1988

Impact Factor: 12.11 · DOI: 10.1021/ja00223a010

work will employ analytical correlated MBPT(2) first- and second-derivative methods[33] to obtain more quantitative results.

Conclusions

1. We have predicted binding energies of BH_3 to HCN, HNC, and CN^-. The bonding of BH_3 to the carbon atom in HCN and CN^- is strongly preferred over the bonding to the nitrogen atom.

2. We have calculated reaction energies for HCN ⇔ HNC, BH_3CN^- ⇔ BH_3NC^-, and $HCNBH_3$ ⇔ $HNCBH_3$ isomerizations. In all cases cyano isomers (i.e. HCN, BH_3CN, and $HCNBH_3$) are more stable than their isocyano isomers. However, the isomerization energy for $H(CN)BH_3$ is much lower than that for the composite molecule, H(CN) (9 and 63 kJ/mol, respectively). This difference results from the much stronger attraction of BH_3 to HNC than to HCN. The calculated equilibrium constant for $HCNBH_3$ ⇔ $HNCBH_3$ is 0.02.

3. Estimated barriers to isomerization are very high in all three reactions (182, 161, and 200 kJ/mol, including ZPE). The calculated barrier for the $H(CN)BH_3$ isomerization is only preliminary. The understanding of the mechanism of this reaction requires a more detailed investigation of the energy hypersurface.

4. The inclusion of effects of electron correlation is inevitable in the quantitative description of the bonding of BH_3 to HCN, HNC, and CN^-. Electron correlation is also very important in the prediction of energies of isomerization but less important in calculations of activation barriers of investigated reactions.

5. We have demonstrated that MBPT methods are suitable for a quantitative prediction of energy characteristics of present isomerization reactions. Higher orders of the wave-function expansion considered in CCSD brought very little change of calculated quantities in comparison to the corresponding SDQ-MBPT(4) values. Even D-MBPT(4), in which only double excitations are taken into account, is quite satisfactory in the present case.

Acknowledgment. M.U. is very grateful for the warm hospitality of Professor R. J. Bartlett and the Quantum Theory Project members during his stay in Gainesville, FL. The authors also thank Professor G. Ryschkewitsch for useful discussions. This work was supported by the USAF Office of Scientific Research.

(33) (a) Harrison, R.; Fitzgerald, G.; Laidig, W. D.; Bartlett, R. J. *Chem. Phys. Lett.* **1986**, *124*, 291. (b) Fitzgerald, G.; Cole, S. J.; Bartlett, R. J. *J. Chem. Phys.* **1986**, *85*, 1701.

Structures and Stabilities of Singly Charged Three-Electron Hemibonded Systems and Their Hydrogen-Bonded Isomers

Peter M. W. Gill and Leo Radom*

Contribution from the Research School of Chemistry, Australian National University, Canberra, A.C.T. 2601, Australia. *Received October 15, 1987*

Abstract: Ab initio molecular orbital theory has been used in a systematic study of the first- and second-row ion dimers $He_2^{\bullet+}$, $(NH_3)_2^{\bullet+}$, $(H_2O)_2^{\bullet+}$, $(HF)_2^{\bullet+}$, $Ne_2^{\bullet+}$, $(PH_3)_2^{\bullet+}$, $(H_2S)_2^{\bullet+}$, $(HCl)_2^{\bullet+}$, and $Ar_2^{\bullet+}$. With the exception of the inert-gas ion dimers, these can exist in principle either as hydrogen-bonded ions or as hemibonded species, the latter involving binding through heavy atom–heavy atom three-electron bonds. The hydrogen-bonded systems are preferred for all the first-row systems, and the two isomers have comparable energies in the case of the $P_2H_6^{\bullet+}$ system, while, for the remaining second-row systems, the hemibonded isomers are preferred. The barriers to interconversion and to dissociation of the hydrogen-bonded and hemibonded isomers are found in most cases to be sufficiently large that, under appropriate conditions, experimental observation of the individual isomers should be possible. A simple Hückel model of the length and strength of a three-electron hemibond is presented and is shown to give a satisfactory qualitative account of such bonding. It is found, nevertheless, that comparatively high levels of ab initio theory, including in particular electron correlation, are necessary to predict accurately the binding energies of hemibonded systems and, in certain cases, to ensure even a *qualitatively* correct description of their potential energy surfaces.

The emergence as stable entities of systems containing a three-electron bond with a formal bond order of $^1/_2$ is an intriguing recent phenomenon. Numerous experimental papers[1-20] on the subject have now appeared, with the pioneering work of Alder[1-4] on nitrogen-containing systems, of Asmus[5-9] on sulfur-containing molecules, and of Symons[10-15] having particular relevance to our own studies. The first theoretical discussions, by Pauling,[21] date from more than 50 years ago. More recently, we have examined a nitrogen-containing system[22] while Clark[23a-c] has reported elegant

(1) Alder, R. W. *Acc. Chem. Res.* **1983**, *16*, 321, and references therein.
(2) Alder, R. W.; Orpen, A. G.; White, J. M. *J. Chem. Soc., Chem. Commun.* **1985**, 949.
(3) Kirste, B.; Alder, R. W.; Sessions, R. B.; Bock, M.; Kurreck, H.; Nelsen, S. F. *J. Am. Chem. Soc.* **1985**, *107*, 2635.
(4) Alder, R. W.; Bonifacic, M.; Asmus, K.-D. *J. Chem. Soc., Perkin Trans. 2* **1986**, 277.
(5) Anklam, E.; Mohan, H.; Asmus, K.-D. *J. Chem. Soc., Chem. Commun.* **1987**, 629.
(6) Bonifacic, M.; Asmus, K.-D. *J. Org. Chem.* **1986**, *51*, 1216, and references therein.
(7) (a) Bonifacic, M.; Weiss, J.; Chaudri, S. A.; Asmus, K.-D. *J. Phys. Chem.* **1985**, *89*, 3910. (b) Mönig, J.; Goslich, R.; Asmus, K.-D. *Ber. Bunsen-Ges. Phys. Chem.* **1986**, *90*, 115. (c) Mahling, S.; Asmus, K.-D.; Glass, R. S.; Hojjatie, M.; Wilson, G. S., submitted for publication.
(8) Göbl, M.; Bonifacic, M.; Asmus, K.-D. *J. Am. Chem. Soc.* **1984**, *106*, 5984, and references therein.
(9) Asmus, K.-D. *Acc. Chem. Res.* **1979**, *12*, 436, and references therein.
(10) Ganghi, N.; Wyatt, J. L.; Symons, M. C. R. *J. Chem. Soc., Chem. Commun.* **1986**, 1424.
(11) Symons, M. C. R.; Wren, B. W.; Muto, H.; Toriyama, K.; Iwasaki, M. *Chem. Phys. Lett.* **1986**, *127*, 424.
(12) Symons, M. C. R.; McConnachie, G. D. G. *J. Chem. Soc., Chem. Commun.* **1982**, 851.
(13) Symons, M. C. R.; Wren, B. W. *J. Chem. Soc., Chem. Commun.* **1982**, 817.
(14) Symons, M. C. R.; Mishra, S. P. *J. Chem. Res., Synop.* **1981**, 214.
(15) Lyons, A. R.; Neilson, G. W.; Symons, M. C. R. *J. Chem. Soc., Chem. Commun.* **1972**, 507.
(16) Gerson, F.; Knöbel, J.; Buser, U.; Vogel, E.; Zehnder, M. *J. Am. Chem. Soc.* **1986**, *108*, 3781.
(17) Nelsen, S. F.; Cunkle, G. T.; Evans, D. H.; Haller, K. J.; Kaftory, M.; Kirste, B.; Kurreck, H.; Clark, T. *J. Am. Chem. Soc.* **1985**, *107*, 3829.
(18) (a) Milicev, S.; Macek, J. *Spectrochim. Acta* **1985**, *41A*, 651. (b) Dinnocenzo, J. P.; Banach, T. E. *J. Am. Chem. Soc.* **1988**, *110*, 971.
(19) Trevor, D. J.; Pollard, J. E.; Brewer, W. D.; Southworth, S. H.; Truesdale, C. M.; Shirley, D. A.; Lee, Y. T. *J. Chem. Phys.* **1984**, *80*, 6083.
(20) Musker, W. K.; Roush, P. B. *J. Am. Chem. Soc.* **1976**, *98*, 3055.
(21) (a) Pauling, L. *J. Am. Chem. Soc.* **1931**, *53*, 3225. (b) Pauling, L. *J. Chem. Phys.* **1933**, *1*, 56.
(22) Bouma, W. J.; Radom, L. *J. Am. Chem. Soc.* **1985**, *107*, 345.

0002-7863/88/1510-4931$01.50/0

studies of systems containing second-row elements and, after completion of the present work, first-row elements.[23d] Additionally, abstract discussions[24,25] of three-electron bonds have sought to elucidate some of the factors responsible for the observed properties of systems containing such bonding.

We define a *three-electron hemibonded* system as one in which a bonding σ molecular orbital between two atoms in a molecule is doubly occupied while the complementary antibonding σ^* molecular orbital is singly occupied. The bond in such a molecule will have a formal bond order of $^1/_2$. The hemibonded three-electron system may be distinguished from (i) *three-electron sesquibonded* systems (e.g. the $C_2H_4^{\bullet+}$ ion) in which all three electrons occupy bonding molecular orbitals so that the formal bond order is $1^1/_2$ and (ii) *one-electron hemibonded* systems (e.g. the $H_2^{\bullet+}$ ion) in which the formal bond order is $^1/_2$ but only one electron is involved in the orbitals in question.

A number of questions concerning hemibonded three-electron systems remain to be answered. We address some of them here with the aid of ab initio molecular orbital calculations on the set of nine dimer cations $He\cdots He^{\bullet+}$, $H_3N\cdots NH_3^{\bullet+}$, $H_2O\cdots OH_2^{\bullet+}$, $HF\cdots FH^{\bullet+}$, $Ne\cdots Ne^{\bullet+}$, $H_3P\cdots PH_3^{\bullet+}$, $H_2S\cdots SH_2^{\bullet+}$, $HCl\cdots ClH^{\bullet+}$, and $Ar\cdots Ar^{\bullet+}$. Of special interest are (a) the stabilities of these systems in their own right and, in particular, with respect to fission of the three-electron bond; (b) the stabilities of the systems relative to their hydrogen-bonded isomers; (c) the stabilities of more general hemibonded systems in which rearrangement to hydrogen-bonded isomers is precluded by substitution (of the potentially hydrogen-bonding hydrogen) and for which substituent effects prove to be of substantial importance (to this end, we have performed calculations on the hemibonded dimer cations of dimethyl ether and of fluoromethanol); and (d) the factors that influence the structure and stability of the three-electron hemibond. These are discussed, making use of qualitative molecular orbital arguments, and the results of the quantitative molecular orbital calculations.

Although our calculations apply strictly only to isolated molecules in the gas phase, they may nevertheless provide information that will be helpful in the interpretation of solution- and solid-phase experiments.

Method and Results

Standard ab initio molecular orbital calculations[26] were carried out with a modified version[27] of the GAUSSIAN 82 system of programs.[28] Initial calculations were performed on prototypical hemibonded dimer cations, represented by the inert-gas ion dimers, at a variety of levels of theory in order to establish a suitable level for the remaining systems. These initial calculations were carried out with a sequence of basis sets (STO-3G, 3-21G, 6-31G, 6-311G(MC),[29] 6-31G**, and 6-311G(MC)**[29]) at the Hartree–Fock (HF) level and with electron correlation incorporated at various orders of Møller–Plesset perturbation theory (MP2, MP3, and MP4). Similar calculations on a prototypical hydrogen-bonded dimer cation ($HFH\cdots F^{\bullet+}$) examined, in addition, the effect of inclusion of diffuse functions in the basis set. On the basis of these results, geometry optimizations for the remaining systems were performed with the split-valence plus d polarization 6-31G* basis set and with electron correlation incorporated via second-order Møller-Plesset perturbation theory. Improved relative energies were obtained for these MP2/6-31G*-optimized structures with the triple-split-valence plus dp polarization 6-311G(MC)**[29] basis set and with use of full fourth-order Møller–Plesset theory. The following additivity approximation was used.

$$\Delta E(\text{MP4/6-311G(MC)**}) \simeq \Delta E(\text{MP4/6-31G*}) + \Delta E(\text{MP2/6-311G(MC)**}) - \Delta E(\text{MP2/6-31G*}) \quad (1)$$

Harmonic vibrational frequencies were calculated at the HF/6-31G* level in order to characterize stationary points as minima (representing

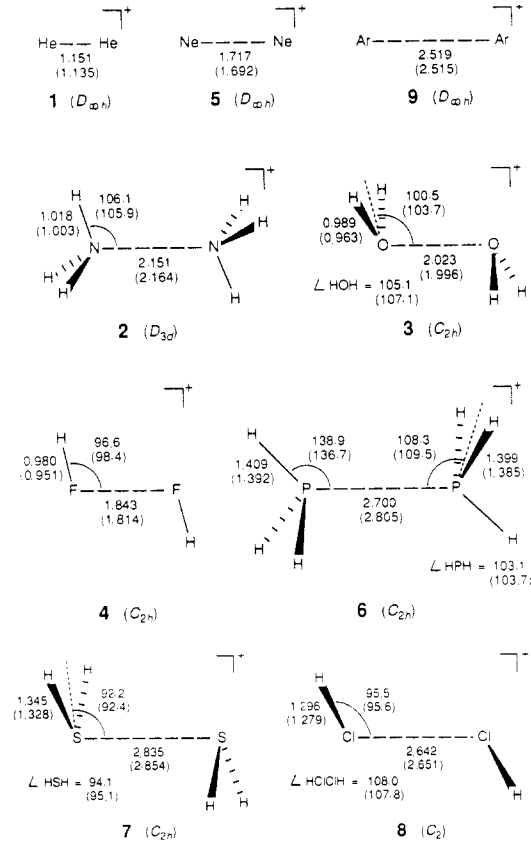

Figure 1. Optimized structures (MP2/6-31G*, with HF/6-31G* values in parentheses) for hemibonded ion dimers. HF/6-31G* results for $H_2O\cdots OH_2^{\bullet+}$ (**3**) and $HF\cdots FH^{\bullet+}$ (**4**) obtained with C_{2h} symmetry constraint (see text).

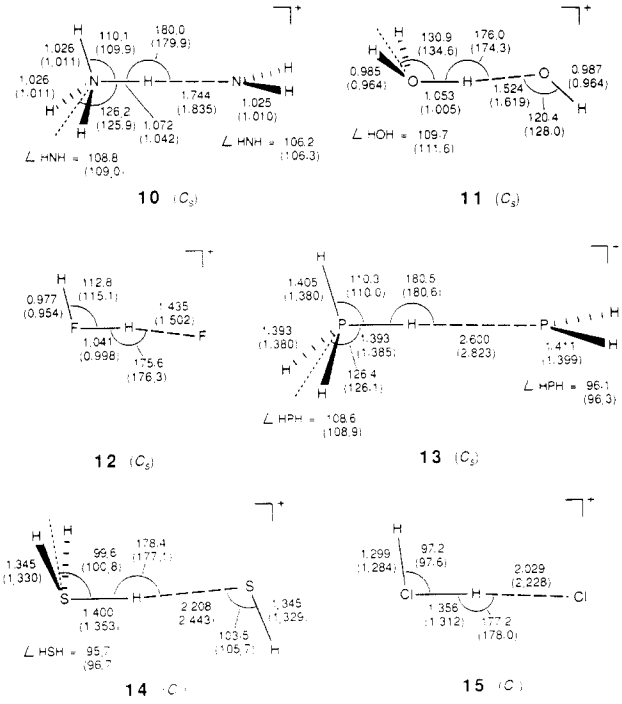

Figure 2. Optimized structures (MP2/6-31G*, with HF/6-31G* values in parentheses) for hydrogen-bonded ion dimers. MP2/6-31G* results for $H_2SH\cdots SH^{\bullet+}$ (**14**) obtained with C_s symmetry constraint (see text).

(23) (a) Clark, T. *J. Comput. Chem.* **1981**, *2*, 261. (b) Clark, T. *J. Comput. Chem.* **1982**, *3*, 112. (c) Clark, T. *J. Comput. Chem.* **1983**, *4*, 404. (d) Clark, T. *J. Am. Chem. Soc.* **1988**, *110*, 1672.

(24) Baird, N. C. *J. Chem. Educ.* **1977**, *54*, 291.

(25) Harcourt, R. D. *J. Chem. Educ.* **1985**, *62*, 99.

(26) For a detailed description of the individual basis sets and correlation procedures, see: Hehre, W. J.; Radom, L.; Schleyer, P. v. R.; Pople, J. A. *Ab Initio Molecular Orbital Theory*; Wiley: New York, 1986.

(27) (a) Baker, J.; Nobes, R. H.; Poppinger, D.; Wong, M. W., unpublished results. (b) Baker, J. *J. Comput. Chem.* **1986**, *7*, 385.

(28) Binkley, J. S.; Frisch, M. J.; DeFrees, D. J.; Raghavachari, K.; Whiteside, R. A.; Schlegel, H. B.; Fluder, E. M.; Pople, J. A. GAUSSIAN 82, Carnegie-Mellon University, Pittsburgh, PA.

(29) The 6-311G(MC)** basis set is based on 6-311G for H, He, and first-row elements and a McLean–Chandler basis set for second-row elements. Polarization function exponents for H and first-row elements are the normal 6-311G** values while those for He and second-row elements are values obtained from optimization of the normal-valent hydrides: Wong, M. W.; Gill, P. M. W.; Nobes, R. H.; Radom, L. *J. Phys. Chem.*, in press.

Table I. Calculated Bond Lengths (r, Å) and Dissociation Energies[a] (ΔE, kJ mol^{-1}) of the Inert-Gas Hemibonded Dimer Cations at Various Levels of Theory

	He···He$^{\bullet+}$		Ne···Ne$^{\bullet+}$		Ar···Ar$^{\bullet+}$	
	r	ΔE	r	ΔE	r	ΔE
UHF/STO-3G	1.159	204	1.557	198	2.392	120
UHF/3-21G	1.153	157	1.656	80	2.568	53
UHF/6-31G	1.135	143	1.717	29	2.586	40
UHF/6-311G	1.108	148	1.733	15	2.571	37
UHF/6-31G**	1.078	181	1.692	38	2.515	47
MP2/6-31G**	1.082	209	1.717	162	2.519	101
MP3/6-31G**[b]	1.086	218	1.708	147	2.524	97
MP4/6-31G**[b]	1.088	222	1.710	155	2.524	99
UHF/6-311G(MC)**	1.069	181	1.722	16	2.468	50
MP2/6-311G(MC)**	1.068	210	1.759	134	2.463	106
MP3/6-311G(MC)**[b]	1.071	218	1.748	116	2.470	100
MP4/6-311G(MC)**[b]	1.073	221	1.755	128	2.471	102
UHF/6-311G(MC)(2d,2p)	1.076	189	1.706	21	2.446	62
MP2/6-311G(MC)(2d,2p)	1.077	217	1.734	144	2.441	121
UHF/6-311G(MC)(df,pd)	1.071	182	1.721	15		
MP2/6-311G(MC)(df,pd)	1.067	213	1.755	135		
MP4/6-311G(MC)(2df,2pd)[c,d]		231		139		117
Huber and Herzberg[e]		238		125		≥100

[a] Without zero-point vibrational contribution. [b] Frozen-core approximation used. [c] Assuming additivity of basis set enhancement and electron correlation effects. [d] MP4/6-311G(MC)(2d,2p) in the case of $Ar_2^{\bullet+}$. [e] See text.

equilibrium structures) or saddle points (representing transition structures) and to evaluate zero-point vibrational energies. The zero-point energies were scaled by 0.9 to account for their overestimation by ~10% at this level of theory. The spin-unrestricted formalism (UHF, UMP) was used for all odd-electron species. The degree of spin contamination, as measured by the deviation of the expectation value ($\langle S^2 \rangle$) of the spin-squared operator from the value of 0.75 required for a pure doublet, was found in all cases to be small.

Optimized structures for the nine hemibonded systems, the six hydrogen-bonded systems, and the six transition structures for interconversion of hemibonded and hydrogen-bonded ions are displayed in Figures 1–3, respectively.

Table I compares calculated bond lengths and dissociation energies of the inert-gas hemibonded dimer cations at various levels of theory. Total energies, zero-point vibrational energies, and $\langle S^2 \rangle$ values for relevant fragment molecules and the dimer cations are listed in Tables II and III, respectively. Relative energies are displayed in Table IV.

Discussion

Theory of the Three-Electron Bond. In the elementary Hückel approximation, the formation of a three-electron bond between two equivalent fragments may be modeled by the perturbative interaction of an appropriate orbital on each of the fragments.[24] Interaction of two fragment orbitals leads to the formation of a bonding and an antibonding molecular orbital, and when overlap is included, the latter is more destabilized than the former is stabilized. For the situation in which both orbitals are doubly occupied, the familiar four-electron repulsion results. However, if the bonding orbital is doubly occupied while the antibonding orbital is only singly occupied, a three-electron bond is formed, and the net energetic stabilization thereby achieved is found to be

$$E_{stab} = [(\alpha + 3\beta)S - \beta - 3\alpha S^2]/(1 - S^2) \quad (2)$$

where, following the usual convention, the symbols α, β, and S represent the Hückel coulomb, resonance, and overlap integrals, respectively. Expression 2 may be simplified further by invoking the Wolfsberg–Helmholtz approximation[30] (eq 3), where K is another empirical constant, to give eq 4.

$$\beta = K\alpha S \quad (3)$$

$$E_{stab} = (K - 1)\alpha S(3S - 1)/(1 - S^2) \quad (4)$$

Inspection of eq 4 shows clearly that the stabilization energy vanishes if the overlap (and hence the resonance integral) is zero, which is to be expected. Furthermore, it is apparent that the three-electron bond energy is also zero when the overlap integral $S = {}^1/_3$. Since α is a negative quantity and K is significantly greater than unity, it follows that E_{stab} is positive for overlaps less than $^1/_3$ and negative for overlaps greater than $^1/_3$. It is not difficult to show by differentiation that the overlap S_0 that leads to the greatest stabilization energy E_0 is given by eq 5, which leads to eq 6.

$$S_0 = 3 - 2(\sqrt{2}) \simeq 0.17 \quad (5)$$

$$E_0 = (\sqrt{2} - {}^3/_2)(K - 1)\alpha \quad (6)$$

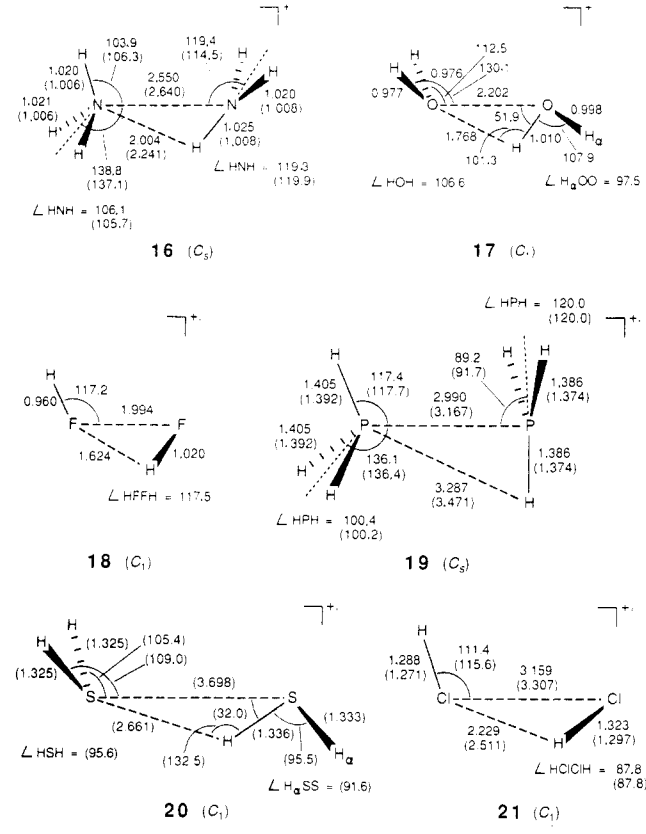

Figure 3. Optimized structures (MP2/6-31G*, with HF/6-31G* values in parentheses) for transition structures linking the hemibonded and hydrogen-bonded systems.

(30) Wolfsberg, M.; Helmholtz, L. *J. Chem. Phys.* **1952**, *20*, 837.

Table II. Calculated Total Energies (Hartrees), Zero-Point Vibrational Energies (ZPVE, kJ mol^{-1}), and $\langle S^2 \rangle$ Values of Fragment Neutrals and Cations[a]

	HF/6-31G*[b]	MP2/6-31G*	MP4/6-31G*[c]	MP2/WGNR[c,d]	ZPVE[e]	$\langle S^2 \rangle$[f]
He	−2.855 16	−2.866 36	−2.869 94	−2.887 42	0.0	
NH_3	−56.184 36	−56.357 38	−56.371 26	−56.408 75	87.4	
H_2O	−76.010 75	−76.199 24	−76.207 33	−76.263 65	54.3	
HF	−100.002 91	−100.184 16	−100.188 43	−100.266 72	23.5	
Ne	−128.474 41	−128.626 18	−128.629 21	−128.731 57	0.0	
PH_3	−342.447 96	−342.562 26	−342.578 31	−342.615 53	61.9	
H_2S	−398.667 32	−398.798 70	−398.812 00	−398.851 42	38.9	
HCl	−460.059 98	−460.202 15	−460.210 88	−460.250 20	17.2	
Ar	−526.773 74	−526.919 99	−526.924 44	−526.957 08	0.0	
$He^{\bullet+}$	−1.993 62	−1.993 62	−1.993 62	−1.998 14	0.0	0.750
$NH_3^{\bullet+}$	−55.873 24	−56.006 94	−56.023 69	−56.049 06	82.7	0.761
$H_2O^{\bullet+}$	−75.615 31	−75.756 95	−75.771 53	−75.814 51	47.5	0.758
$HF^{\bullet+}$	−99.489 60	−99.618 92	−99.630 12	−99.689 94	17.0	0.755
$Ne^{\bullet+}$	−127.751 71	−127.849 40	−127.857 45	−127.950 59	0.0	0.752
$PH_3^{\bullet+}$	−342.131 56	−342.223 94	−342.236 97	−342.270 50	62.0	0.757
$H_2S^{\bullet+}$	−398.326 99	−398.435 79	−398.449 99	−398.483 30	38.3	0.762
$HCl^{\bullet+}$	−459.633 97	−459.752 03	−459.763 38	−459.795 53	15.8	0.757
$Ar^{\bullet+}$	−526.235 04	−526.356 02	−526.364 56	−526.389 71	0.0	0.755
HeH^+	−2.909 87	−2.926 72	−2.931 79	−2.961 21	17.3	
NH_4^+	−56.530 77	−56.703 58	−56.718 61	−56.755 04	125.9	
H_3O^+	−76.289 34	−76.477 61	−76.486 87	−76.547 99	86.8	
H_2F^+	−100.197 82	−100.383 31	−100.388 38	−100.468 08	47.3	
NeH^+	−128.550 16	−128.709 90	−128.713 62	−128.816 15	15.4	
PH_4^+	−342.761 58	−342.871 06	−342.886 76	−342.927 77	91.7	
H_3S^+	−398.941 84	−399.073 29	−399.089 21	−399.132 56	68.5	
H_2Cl^+	−460.266 88	−460.412 58	−460.424 53	−460.471 29	39.8	
ArH^+	−526.900 78	−527.052 90	−527.060 54	−527.105 28	15.5	
$NH_2^{\bullet}$	−55.557 70	−55.693 75	−55.710 06	−55.732 59	48.6	0.758
$OH^{\bullet}$	−75.382 28	−75.523 21	−75.536 15	−75.572 76	21.5	0.756
$F^{\bullet}$	−99.364 96	−99.489 04	−99.498 65	−99.554 17	0.0	0.753
$PH_2^{\bullet}$	−341.849 60	−341.945 79	−341.959 16	−341.987 42	34.5	0.763
$SH^{\bullet}$	−398.064 40	−398.172 09	−398.183 21	−398.211 22	15.6	0.758
$Cl^{\bullet}$	−459.447 96	−459.562 06	−459.569 83	−459.593 34	0.0	0.755

[a] MP2/6-31G*-optimized structures unless otherwise noted. [b] HF/6-31G*-optimized structures. [c] Frozen-core approximation used. [d] 6-311G(MC)** basis set used.[29] [e] HF/6-31G*//HF/6-31G* values, scaled by 0.9. [f] Spin-squared expectation values.

Table III. Calculated Total Energies (Hartrees), Zero-Point Vibrational Energies (ZPVE, kJ mol^{-1}), and $\langle S^2 \rangle$ Values of the Hemibonded and Hydrogen-Bonded $X_2^{\bullet+}$ Systems[a] and of the Transition Structures Linking Them[b]

$X_2^{\bullet+}$		HF/6-31G*[c]	MP2/6-31G*	MP4/6-31G*[d]	MP2/WGNR[d,e]	ZPVE[f]	$\langle S^2 \rangle$[g]
He–He$^{\bullet+}$	**1**	−4.903 17	−4.922 61	−4.931 20	−4.963 10	8.2	0.761
H_3N–$NH_3^{\bullet+}$	**2**	−112.096 13	−112.428 53	−112.457 23	−112.518 44	185.8	0.775
H_3NH–$NH_2^{\bullet+}$	**10**	−112.124 10	−112.437 71	−112.467 80	−112.527 76	184.0	0.759
TS: **2** → **10**	**16**	−112.091 76	−112.406 31	−112.436 93	−112.497 92	179.1	0.762
H_2O–$OH_2^{\bullet+}$	**3**	−151.662 54[h]	−152.030 24	−152.048 98	−152.147 50	114.7[i]	0.775
H_2OH–$OH^{\bullet+}$	**11**	−151.704 47	−152.039 42	−152.060 64	−152.159 23	114.7	0.757
TS: **3** → **11**	**17**	*j*	−152.008 51	−152.031 35	−152.129 07	109.8[k]	0.759
HF–$FH^{\bullet+}$	**4**	−199.524 26[h]	−199.879 96	−199.890 76	−200.025 26	50.8[i]	0.769
HFH–$F^{\bullet+}$	**12**	−199.579 43	−199.894 56	−199.909 03	−200.041 09	50.8	0.754
TS: **4** → **12**	**18**	*j*	−199.850 77	−199.867 60	−199.998 56	44.4[k]	0.756
Ne–$Ne^{\bullet+}$	**5**	−256.240 64	−256.537 40	−256.545 55	−256.732 72	3.5	0.764
H_3P–$PH_3^{\bullet+}$	**6**	−684.610 29	−684.829 76	−684.858 11	−684.929 67	133.3	0.773
H_3PH–$PH_2^{\bullet+}$	**13**	−684.620 24	−684.828 62	−684.857 10	−684.926 47	129.8	0.763
TS: **6** → **13**	**19**	−684.590 25	−684.808 15	−684.836 73	−684.907 24	127.0	0.771
H_2S–$SH_2^{\bullet+}$	**7**	−797.026 11	−797.282 53	−797.309 07	−797.382 73	90.1	0.773
H_2SH–$SH^{\bullet+}$	**14**	−797.018 94	−797.263 13[l]	−797.289 47	−797.363 18	88.0	0.759
TS: **7** → **14**	**20**	−797.008 39	*j*	*j*	*j*	82.0	0.762[c]
HCl–$ClH^{\bullet+}$	**8**	−919.721 83	−920.001 25	−920.020 24	−920.093 65	41.0	0.767
HClH–$Cl^{\bullet+}$	**15**	−919.723 95	−919.988 59	−920.007 70	−920.081 24	42.3	0.756
TS: **8** → **15**	**21**	−919.707 30	−919.972 96	−919.992 65	−920.065 41	36.3	0.758
Ar–$Ar^{\bullet+}$	**9**	−1053.026 82	−1053.314 58	−1053.326 72	−1053.386 51	1.5	0.764

[a] Electronic states examined were $^2\Sigma_u$ (**1**), $^2A_{2u}$ (**2**), ^2B_u (**3**), ^2B_u (**4**), $^2\Sigma_u$ (**5**), $^2A_{2u}$ (**6**), ^2B_u (**7**), ^2B (**8**), $^2\Sigma_u$ (**9**), $^2A'$ (**10**), $^2A''$ (**11**), $^2A''$ (**12**), $^2A'$ (**13**), $^2A''$ (**14**), and $^2A''$ (**15**). [b] MP2/6-31G*-optimized structures, unless otherwise noted. [c] HF/6-31G*-optimized structures. [d] Frozen-core approximation used. [e] 6-311G(MC)** basis set used.[29] [f] HF/6-31G*//HF/6-31G* values scaled by 0.9, unless otherwise noted. [g] Spin-squared expectation values. [h] Symmetry constrained to C_{2h}; one (**4**) or two (**3**) imaginary frequencies at this level of theory. [i] Assumed equal to that of the H-bonded isomer. [j] Not relevant at this level of theory. [k] MP2/3-21G//MP2/3-21G value, scaled by 0.93. [l] Symmetry constrained to C_s; one imaginary frequency at this level of theory.

The predicted value for S_0 from this crude model is of special interest because it is entirely independent of any of the empirical Hückel parameters. The overlap is of a σ rather than a π type, and, as such, an overlap integral of 0.17 is rather small. (By

Table IV. Calculated Relative Energies (kJ mol^{-1})[a]

	HF/6-31G*[b]	MP2/6-31G*	MP4/6-31G*[c]	MP2/WGNR[c,d]	MP4/WGNR[d,e]	MP4/WGNR[d,f]
$He-He^{\bullet+}$ (**1**)	0	0	0	0	0	0
$He + He^{\bullet+}$	143	164	178	204	217	209
$H_3N-NH_3^{\bullet+}$ (**2**)	0	0	0	0	0	0
$H_3NH-NH_2^{\bullet+}$ (**10**)	−73	−24	−28	−24	−28	−30
TS: **2** → **10** (**16**)	11	58	53	54	49	42
$NH_3 + NH_3^{\bullet+}$	101	169	164	159	154	138
$NH_4^+ + NH_2^{\bullet}$	20	82	75	81	74	63
$H_2O-OH_2^{\bullet+}$ (**3**)	0	0	0	0	0	0
$H_2OH-OH^{\bullet+}$ (**11**)	−110[g]	−24	−31	−31	−37	−37
TS: **3** → **11** (**17**)	*g*	57	46	48	38	33
$H_2O + H_2O^{\bullet+}$	96	194	184	182	172	159
$H_3O^+ + OH^{\bullet}$	−24	77	68	70	61	55
$HF-FH^{\bullet+}$ (**4**)	0	0	0	0	0	0
$HFH-F^{\bullet+}$ (**12**)	−145[g]	−38	−48	−42	−51	−51
TS: **4** → **12** (**18**)	*g*	77	61	70	54	48
$HF + HF^{\bullet+}$	83	202	190	180	168	158
$H_2F^+ + F^{\bullet}$	−101	20	10	8	−2	−6
$Ne-Ne^{\bullet+}$ (**5**)	0	0	0	0	0	0
$Ne + Ne^{\bullet+}$	38	162	155	133	125	122
$H_3P-PH_3^{\bullet+}$ (**6**)	0	0	0	0	0	0
$H_3PH-PH_2^{\bullet+}$ (**13**)	−26	3	3	8	8	5
TS: **6** → **13** (**19**)	53	57	56	59	58	52
$PH_3 + PH_3^{\bullet+}$	81	114	112	115	113	103
$PH_4^+ + PH_2^{\bullet}$	−2	34	32	38	36	29
$H_2S-SH_2^{\bullet+}$ (**7**)	0	0	0	0	0	0
$H_2SH-SH^{\bullet+}$ (**14**)	19	51[g]	51[g]	51[g]	52[g]	50[g]
TS: **7** → **14** (**20**)	47	*h*	*h*	*h*	*h*	*h*
$H_2S + H_2S^{\bullet+}$	83	126	124	126	124	111
$H_3S^+ + SH^{\bullet}$	52	98	96	102	101	95
$HCl-ClH^{\bullet+}$ (**8**)	0	0	0	0	0	0
$HClH-Cl^{\bullet+}$ (**15**)	−6	33	33	33	32	34
TS: **8** → **15** (**21**)	38	74	72	74	72	68
$HCl + HCl^{\bullet+}$	73	124	121	126	123	115
$H_2Cl^+ + Cl^{\bullet}$	18	70	68	76	74	73
$Ar-Ar^{\bullet+}$ (**9**)	0	0	0	0	0	0
$Ar + Ar^{\bullet+}$	47	101	99	104	102	101

[a] MP2/6-31G*-optimized structures unless otherwise noted. [b] HF/6-31G*-optimized structures. [c] Frozen-core approximation used. [d] 6-311G-(MC)** basis set used.[29] [e] Additivity approximation given by eq 1 used. [f] Including zero-point vibrational contribution. [g] First-order saddle point at the level of theory used for geometry optimization (see text). [h] Not relevant at this level of theory.

comparison, the carbon p_σ overlap integral in ethane, using the minimal STO-3G basis set, is 0.31). This suggests that three-electron hemibonds are likely to be substantially longer than normal two-electron bonds. In fact, the abnormally long three-electron N–N bond in $H_3N\cdots NH_3^{\bullet+}$ (2.164 Å) was noted by Bouma and Radom,[22] who contrasted it with the two-electron bond in the doubly charged $H_3N-NH_3^{2+}$ (1.442 Å). Subsequent experimental X-ray crystal structure determinations provided strong confirmation of long three-electron N–N bonds with values of 2.295 and 2.160 Å.[2,16] It is interesting to note that when the STO-3G basis set is used, the magnitude of the nitrogen p_σ overlap integral in $H_3N\cdots NH_3^{\bullet+}$ is 0.15 (see Table V below), which is remarkably close to the Hückel prediction.

The maximum binding energy of the three-electron hemibond appears, from eq 6, to be proportional to the coulomb integral of the component atomic orbitals. This observation leads to the prediction that the strongest homonuclear three-electron bonds ought to be formed between highly electronegative atoms. Of the nine model systems considered here, $He\cdots He^{\bullet+}$ is therefore predicted to be the most strongly bonded, while $H_3P\cdots PH_3^{\bullet+}$ should be the most weakly bound.

Hemibonded Systems. Each of the nine hemibonded systems has been previously examined theoretically, at various levels of approximation. We[22] have investigated the hydrazinium radical cation $N_2H_6^{\bullet+}$; Ortiz[31] has examined both of the isomers of $H_4S_2^{\bullet+}$; while Clark[23] has studied the $P_2H_6^{\bullet+}$, $H_4S_2^{\bullet+}$ and $H_2Cl_2^{\bullet+}$ species and more recently the $N_2H_6^{\bullet+}$, $H_4O_2^{\bullet+}$, $H_2F_2^{\bullet+}$, $Ne_2^{\bullet+}$, and $Ar_2^{\bullet+}$ systems. The helium dimer cation $He_2^{\bullet+}$ has been the subject of many papers,[21,32-40] beginning with Pauling's[21] seminal work in

Table V. Correlation of Dissociation Energy (E_{diss}, kJ mol^{-1})[a] and Overlap Integral (S)[b] of Hemibonded Dimer Cations ($X_2^{\bullet+}$) with HOMO Energy of X (E_{HOMO}, Hartrees)[c]

X	$E_{HOMO}(X)$	$E_{diss}(X_2^{\bullet+})$	$S(X_2^{\bullet+})$
He	−0.91	209	0.23
NH_3	−0.42	138	0.15
H_2O	−0.50	159	0.13
HF	−0.63	158	0.11
Ne	−0.83	122	0.09
PH_3	−0.38	103	0.15
H_2S	−0.38	111	0.13
HCl	−0.48	115	0.13
Ar	−0.59	101	0.11

[a] MP4/6-311G(MC)**//MP2/6-31G* with zero-point correction. [b] STO-3G//STO-3G values. [c] HF/6-31G*//HF/6-31G* values.

(31) Ortiz, J. V. *Chem. Phys. Lett.* **1987**, *134*, 366.
(32) Clary, D. C. *Mol. Phys.* **1977**, *34*, 793.
(33) Liu, B. *Phys. Rev. Lett.* **1971**, *27*, 1251.
(34) Khan, A.; Jordan, K. D. *Chem. Phys. Lett.* **1986**, *128*, 368.
(35) Gilbert, T. L.; Wahl, A. C. *J. Chem. Phys.* **1971**, *55*, 5247.
(36) Ermler, W. C.; Mulliken, R. S.; Wahl, A. C. *J. Chem. Phys.* **1977**, *66*, 3031.
(37) Buenker, R. J.; Peyerimhoff, S. D.; Butscher, W. *Mol. Phys.* **1978**, *35*, 771.
(38) Rai Dastidar, T. K.; Rai Dastidar, K. *Chem. Phys. Lett.* **1982**, *85*, 229.
(39) Rai Dastidar, T. K.; Rai Dastidar, K.; Sen Gupta, R. *Chem. Phys. Lett.* **1983**, *96*, 85.
(40) Van Lenthe, J. H.; Balint-Kurti, G. G. *J. Chem. Phys.* **1983**, *78*, 5699.

the 1930s and culminating in a revealing Hylleraas-type calculation by Clary,[32] a large CI calculation by Liu,[33] and an MCSCF study by Khan and Jordan.[34] Gilbert and Wahl[35] have found single-configuration wave functions for $He_2^{\bullet+}$, $Ne_2^{\bullet+}$, and $Ar_2^{\bullet+}$, Michels et al.[41] and Wadt[42] have investigated the $Ne_2^{\bullet+}$, $Ar_2^{\bullet+}$, $Kr_2^{\bullet+}$, and $Xe_2^{\bullet+}$ systems, and Christiansen et al.[43] have examined $Ar_2^{\bullet+}$, $Kr_2^{\bullet+}$, and $Xe_2^{\bullet+}$. It seems appropriate, therefore, to draw together these diverse systems and to examine, *at a uniform and adequate level of theory*, the hemibonds present in all of them.

To begin, it is useful to examine the performance of a range of different levels of theory in describing the three-electron bond. Clearly, it is desirable, if possible, to conduct such an investigation on a small number of prototypical systems, and the inert-gas dimer radical cations $He_2^{\bullet+}$, $Ne_2^{\bullet+}$, and $Ar_2^{\bullet+}$ were selected for this purpose. Because of the structural simplicity of these species, calculations may be performed at comparatively high levels of theory. In this way, it is hoped, an estimate of the reliability of the less sophisticated levels of theory may be gauged.

The helium–helium, neon–neon, and argon–argon bond lengths were optimized and corresponding dissociation energies calculated at several progressively more accurate theoretical levels (Table I). Huber and Herzberg[44] quote the theoretical $D_e(He_2^{\bullet+})$ calculated by Liu[33] (2.469 eV, 238 kJ mol^{-1}) as the best available estimate of this quantity. For $Ne_2^{\bullet+}$ and $Ar_2^{\bullet+}$ they recommend the experimental values $D_e(Ne_2^{\bullet+})$ = 1.30 eV (125 kJ mol^{-1}) and $D_0(Ar_2^{\bullet+}) \geq$ 1.049 eV (101 kJ mol^{-1}). The difference between $D_0(Ar_2^{\bullet+})$ and $D_e(Ar_2^{\bullet+})$ is approximately 1 kJ mol^{-1} (Table III). If the D_e values in Table I are compared both with these reference values and with one another, a number of important features of the ab initio description of three-electron hemibonds become apparent:

(1) At the Hartree–Fock level, small basis sets (e.g. STO-3G) generally give substantially larger dissociation energies than larger sets.

(2) Polarization functions lead to a shortening and strengthening of the hemibonds.

(3) The improvement in using a triple- rather than a double-split-valence basis set is quite small for He···He$^{\bullet+}$ and Ar···Ar$^{\bullet+}$ but significant for Ne···Ne$^{\bullet+}$ where it is associated with an increase in bond length of 0.042 Å and a decrease in dissociation energy of 28 kJ mol^{-1} at the MP2 level.

(4) Large basis set Hartree–Fock calculations yield dissociation energies that significantly underestimate the true values. In the cases of $Ne_2^{\bullet+}$ and $Ar_2^{\bullet+}$ this effect is particularly marked.

(5) Incorporation of electron correlation is essential in order to describe satisfactorily the dissociation energies of these systems.

(6) Most of the correlation effects are well described by second-order perturbation theory (MP2).

(7) Assuming the additivity of basis set enhancement and electron correlation effects, we can use the results of Table I to estimate MP4/6-311G(MC)(2df,2pd) values (MP4/6-311G(MC)(2d,2p) in the case of $Ar_2^{\bullet+}$) of $D_e(He_2^{\bullet+})$ = 231 kJ mol^{-1}, $D_e(Ne_2^{\bullet+})$ = 139 kJ mol^{-1}, and $D_e(Ar_2^{\bullet+})$ = 117 kJ mol^{-1}. These lead us to suggest that the experimental dissociation energies quoted above for $Ne_2^{\bullet+}$ and $Ar^{2\bullet+}$ are possibly slightly too low.

On the basis of these observations and on the assumption that the behavior of other hemibonded systems would be similar, it would seem that a theoretical level suitable for geometry optimizations should include at least a double-split-valence basis set with polarization functions on heavy atoms but not necessarily on hydrogen. We believe, furthermore, that the use of an uncorrelated level of theory (e.g. HF/6-31G*) may be unreliable in reproducing even the gross qualitative features of certain of the potential surfaces. In particular, since the Hartree–Fock well depths for some of these systems are greatly underestimated, the study of the interconversions of hemibonded systems with their hydrogen-bonded isomers *must* be conducted at a correlated level. Indeed, we shall see that, for the HF···FH$^{\bullet+}$ and H_2O···$OH_2^{\bullet+}$ systems, the Hartree–Fock description of the potential surfaces is somewhat misleading. We therefore chose MP2/6-31G* as our optimization level. Improved relative energies may then be obtained via single-point calculations at the MP4/6-311G(MC)** level. This approach seems to provide a satisfactory compromise between economy and accuracy.

It is also amusing to note that because of a fortuitous cancellation of errors associated with basis set truncation and neglect of correlation, the simplest of all of the models in Table I, namely HF/STO-3G, gives surprisingly good estimates of hemibond dissociation energies.

Having chosen a theoretical level at with optimizations may be carried out and after performing MP4/6-311G(MC)** single-point energy calculations (Tables II and III) and obtaining relative energies (Table IV), we may compare relevant results (Table V) with the predictions of the qualitative Hückel model described above.

The first of these predictions was that the overlap integral S in the hemibonded dimer should be roughly 0.17. Although S is clearly dependent on the nature of X, it can be seen from Table V that the crude Hückel prediction is remarkably good.

The qualitative model also predicts that the dissociation energy of the three-electron hemibond should be large when α, the Hückel coulomb integral, is numerically large. The energy of the highest occupied molecular orbital (E_{HOMO}) of the monomer X varies roughly in proportion to α, and hence we expect a correlation between the middle two columns of Table V. That such a correlation is roughly observed leads us to believe that although correlated treatments are necessary for a quantitative understanding of the three-electron hemibond, the qualitative features are well described by the simplest possible molecular orbital picture.

The dissociation energies summarized in Table V demonstrate that three-electron hemibonds are rather strong. More than 100 kJ mol^{-1} are required to break even the weakest bonds studied (those found in H_3P···$PH_3^{\bullet+}$ and Ar···Ar$^{\bullet+}$). This suggests that, unless the possibility of internal rearrangement to a more stable isomer precludes it, each of the nine hemibonded systems studied should be experimentally observable. Of the various conceivable rearrangements, the most likely seem to be those to hydrogen-bonded isomers.

Hydrogen-Bonded Systems. Of the six molecules in this paper for which hydrogen bonding is possible, four have previously been examined theoretically. Lathan et al.,[45] Cao et al.[46] Tomoda and Kimura,[47] and Bouma and Radom[22] have investigated the hydrogen-bonded isomer of the ammonia dimer radical cation H_3NH···$NH_2^{\bullet+}$ (**10**). Lathan et al.,[45] Clark and Cromarty,[48] Moncrieff et al.,[49] Tomoda et al.,[50] and Curtiss[51] have all performed calculations on the water dimer radical cation H_2O-H···$OH^{\bullet+}$ (**11**), a molecule of considerable interest both theoretically and experimentally. The hydrogen fluoride dimer radical cation HFH···$F^{\bullet+}$ (**12**) has received much less attention. Indeed, we are aware of only two previous studies of it and, in both, Lathan et al.[45] and Peel[52] examined the molecule using only modest levels

(41) Michels, H. H.; Hobbs, R. H.; Wright, L. A. *J. Chem. Phys.* **1978**, *69*, 5151.
(42) (a) Wadt, W. R. *J. Chem. Phys.* **1978**, *68*, 402. (b) Wadt, W. R. *J. Chem. Phys.* **1980**, *73*, 3915.
(43) Christiansen, P. A.; Pitzer, K. S.; Lee, Y. S.; Yates, J. H.; Ermler, W. C.; Winter, N. W. *J. Chem. Phys.* **1981**, *75*, 5410.
(44) Huber, K. P.; Herzberg, G. *Molecular Spectra and Molecular Structure IV. Constants of Diatomic Molecules*; Van Nostrand Reinhold: New York, 1979.
(45) Lathan, W. A.; Curtiss, L. A.; Hehre, W. J.; Lisle, J. B.; Pople, J. A. *Prog. Phys. Org. Chem.* **1974**, *11*, 175.
(46) Cao, H. Z.; Evleth, E. M.; Kassab, E. *J. Chem. Phys.* **1984**, *81*, 1512.
(47) (a) Tomoda, S.; Kimura, K. *Chem. Phys. Lett.* **1985**, *121*, 159. (b) Tomoda, S. *Chem. Phys.* **1986**, *110*, 431.
(48) Clark, D. T.; Cromarty, B. J. *Theoret. Chim. Acta* **1977**, *44*, 181.
(49) Moncrieff, D.; Hillier, H.; Saunders, V. R. *Chem. Phys. Lett.* **1982**, *89*, 447.
(50) (a) Tomoda, S.; Achiba, Y.; Kimura, K. *Chem. Phys. Lett.* **1982**, *87*, 197. (b) Sato, K.; Tomoda, S.; Kimura, K. *Chem. Phys. Lett.* **1983**, *95*, 579. (c) Tomoda, S.; Kimura, K. *Chem. Phys.* **1983**, *82*, 215. (d) Tomoda, S.; Kimura, K. *Chem. Phys. Lett.* **1983**, *102*, 560. (e) Tomoda, S.; Kimura, K. *Chem. Phys. Lett.* **1983**, *111*, 434.
(51) (a) Curtiss, L. A. *Chem. Phys. Lett.* **1983**, *96*, 442. (b) Curtiss, L. A. *Chem. Phys. Lett.* **1984**, *112*, 409.

Table VI. Calculated Hydrogen-Bond Length (Å) and Dissociation Energy[a] (E_{diss}, kJ mol^{-1}) of HFH···F$^{\bullet+}$ (^{2}A″) at Various Levels of Theory

	H-bond length	E_{diss}
HF/3-21G	1.424	70
HF/6-31G*	1.502	44
MP2/6-31G*	1.435	58
MP3/6-31G*[b]	1.451	56
MP4/6-31G*[b]	1.445	58
HF/6-31G**	1.484	43
MP2/6-31G**	1.393	61
HF/6-31+G*	1.530	35
MP2/6-31+G*	1.458	45
HF/6-31++G*	1.531	35
HF/6-311G(MC)*	1.613	32
MP2/6-311G(MC)*	1.547	42
HF/6-311G(MC)**	1.502	33
HF/6-311+G(MC)*	1.616	28
MP2/6-311+G(MC)*	1.548	37

[a] Fully optimized but without zero-point vibrational contribution. [b] Frozen-core approximation used.

of theory. We are unaware of any previous theoretical studies of either the hydrogen-bonded phosphine dimer cation H_3P-H···$PH_2^{\bullet+}$ (**13**) or the hydrogen chloride dimer cation HClH···Cl$^{\bullet+}$ (**15**). Ortiz et al.[31,53] have performed calculations on the hydrogen-bonded hydrogen sulfide dimer cation H_2SH···$SH^{\bullet+}$ (**14**).

In many of these studies, the theoretical levels used were of qualitative rather than quantitative value. In only a few were structural optimizations conducted with better than split-valence quality basis sets, and in none were any structures determined at a correlated level of theory. In that *correlated optimizations using polarization basis sets* have been used in the present calculations, they represent a significant improvement on any of those preceding them.

Furthermore, we are not aware of any ab initio studies of any of the transition structures linking the hemibonded and hydrogen-bonded isomers considered in this paper. We believe, however, that establishing good estimates of the barriers to these interconversions is of critical importance in any attempt to understand the stability (or otherwise) of the hydrogen-containing systems.

As we did for the hemibonded systems, it is useful to begin by making a critical assessment of the description of hydrogen bonding in cationic species afforded by a range of different levels of theory. For simplicity, the hydrogen fluoride dimer cation (**12**) was selected and the length of its hydrogen bond and its dissociation energy determined at several theoretical levels (Table VI). In recent definitive studies of basis set and correlation effects in neutral[54a] and protonated[54b] hydrogen-bonded dimers of NH_3, H_2O, and HF, Del Bene found that the presence of diffuse functions on heavy atoms in the basis set significantly reduces the dissociation energies of such species. She found also that electron correlation was important in stabilizing the hydrogen bonds in these molecules. It is useful to compare these observations with the data in Table VI and to examine the ab initio description of the type of hydrogen-bonded cations that are considered in this paper.

(1) At the Hartree-Fock level, small basis sets (e.g. 3-21G) generally give larger dissociation energies than larger sets.

(2) Polarization functions on hydrogen atoms shorten the length, but have only a small effect on the strength, of the hydrogen bond.

(3) The addition of diffuse functions on heavy atoms to a double-split-valence basis set or the use of a triple-split-valence rather than a double-split-valence basis set have similar effects. Both lead to a lengthening and weakening of the hydrogen bond. Furthermore, the effects of augmenting a triple-split-valence basis set with diffuse functions are small.

(4) Incorporation of electron correlation substantially shortens and strengthens the hydrogen bond.

(5) Most of the correlation effects are well described by second-order perturbation theory (MP2).

On the basis of these observations and on the assumption that the behavior of the other hydrogen-bonded systems would be similar, we decided that the theoretical level chosen for optimizing the hemibonded systems (MP2–6-31G*) would also be suitable for the geometry optimizations of the hydrogen-bonded systems and that single-point energy calculations could then be performed at the MP4/6-311G(MC)** level. In choosing the same levels of theory at which to treat the hemibonded systems, their hydrogen-bonded isomers, and, furthermore, the transition structures linking them, we are treating each of the nine potential surfaces considered in this paper as uniformly as possible.

Tomoda and Kimura[47b] have successfully rationalized the discrepancies between the experimental and calculated ionization energies of the hydrogen-bonded H_3N···HNH_2 and H_2O···HOH species through a careful consideration of the geometry changes that take place when these molecules are ionized. However, although it is such ionization (or appearance) energies, rather than dissociation energies, that are usually measured experimentally, the primary concern of the present paper is to examine the structures and stabilities of the dimer cations, and, consequently, we will not consider ionization processes here.

Some of the salient structural and energetic features of the hydrogen-bonded systems are summarized in Table VII. The two dissociation processes examined for each molecule are those defined by Tomoda and Kimura[47a] as the "protonation channel" and the "nonprotonation channel". In the protonation channel, which is always the more facile of the two decomposition modes, the hydrogen bond simply breaks thereby completing the proton transfer, which occurs spontaneously when the dimer cation is formed from two monomer units. In the nonprotonation channel, the proton is first returned to the monomer from which it originated and only then does the dimer fragment. Upon comparison of the two E_{diss} columns of Table VII, it is clear that the nonprotonation reaction is not likely to compete significantly with the protonation channel, except (possibly) in the case of H_2SH···$SH^{\bullet+}$.

The tendency for the length of the hydrogen bond to diminish as the heavy atom becomes more electronegative is marked, but although the bonds in the halogen-containing compounds are the shortest, they are not the strongest. Indeed, apart from the observation that hydrogen bonds to nitrogen and oxygen are particularly strong, it is difficult to discern any simple trends in the dissociation energies of Table VII.

We conclude by noting that all the hydrogen-bonded systems have significant barriers to dissociation and, aside from the possibility of rearrangement to their hemibonded isomers, they should all be observable under appropriate experimental conditions. The first-row hydrogen-bonded dimer cations tend to be more strongly bound than the second-row systems. The rearrangement barriers are clearly of critical importance in assessing the stabilities of the hemibonded and hydrogen-bonded ions and these are examined in the following sections.

$N_2H_6^{\bullet+}$ System. The potential surface of the ammonia dimer radical cation is depicted schematically in Figure 4a. The hemibonded ion H_3N···$NH_3^{\bullet+}$ (**2**) is metastable, lying 30 kJ mol^{-1} higher in energy than the isomeric hydrogen-bonded species H_3NH···$NH_2^{\bullet+}$ (**10**). However, the barrier to its isomerization is 42 kJ mol^{-1}, which suggests that the hemibonded system might be observable in an experiment of sufficiently small time scale. Indeed, very recently, Symons et al.[10] announced that they had observed the ESR spectrum of free H_3N···$NH_3^{\bullet+}$ formed by electron capture by the hydrazinium salt [$N_2H_6^{2+}SO_4^{2-}$] at 77 K. They also comment that the p/s character ratio of approximately 7.5 on the nitrogen atoms indicates that the two NH_3 units must be nearly planar. Our calculated structure (**2**, Figure 1) confirms that the NH_3 units in H_3N···$NH_3^{\bullet+}$ are distorted toward planarity by roughly 6° compared with free NH_3.

(52) Peel, J. B. *Int. J. Quantum Chem.* **1983**, *23*, 653.
(53) Fernandez, P. F.; Ortiz, J. V.; Walters, E. A. *J. Chem. Phys.* **1986**, *84*, 1653.
(54) (a) Del Bene, J. E. *J. Chem. Phys.* **1987**, *86*, 2110. (b) Del Bene, J. E. *J. Comput. Chem.* **1987**, *8*, 810.

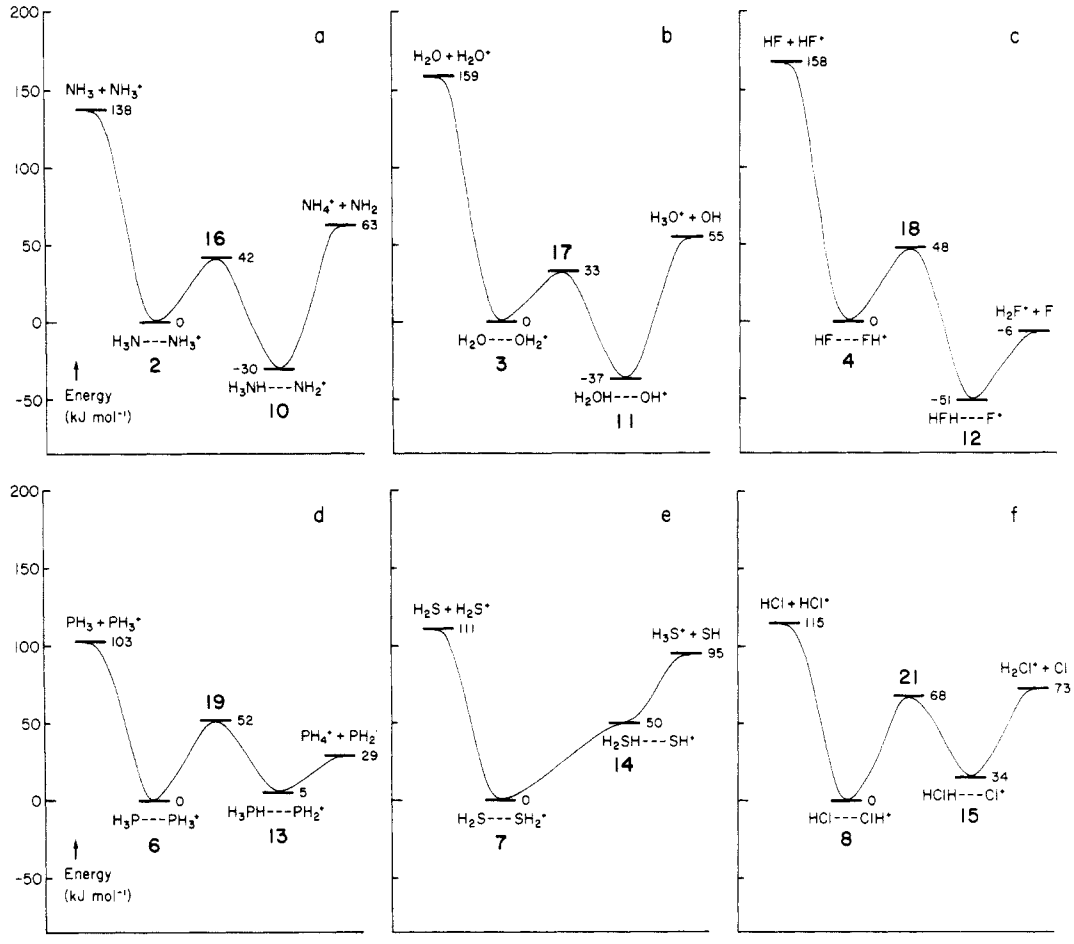

Figure 4. Schematic potential energy surfaces showing rearrangement and dissociative processes for hemibonded and hydrogen-bonded ion dimers: (a) $(NH_3)_2^{\bullet+}$, (b) $(H_2O)_2^{\bullet+}$, (c) $(HF)_2^{\bullet+}$, (d) $(PH_3)_2^{\bullet+}$, (e) $(H_2S)_2^{\bullet+}$, and (f) $(HCl)_2^{\bullet+}$.

It has been noted[47] that the structures of the neutral and singly ionized forms of the hydrogen-bonded ammonia dimer are strikingly different. Specifically, a spontaneous proton transfer takes place when an electron is removed from the neutral dimer so that, as Tomoda and Kimura[47] write, the hydrogen-bonded ammonia dimer cation may be viewed "as a complex between the ammonium ion (NH_4^+) and the aminyl radical ($NH_5^{\bullet}$)". We confirm that the hydrogen bond in **10** is essentially linear. It is interesting also to note that, in the transition structure **16** for isomerization of **2** to **10**, the proton transfer has barely begun, the relevant N–H bond having stretched by only 0.007 Å.

The N–N bond in the hemibonded isomer **2** is surprisingly strong despite its length. Although the nitrogen atoms are more than 2 Å apart (Figure 1) and the overlap is only 0.15 Å (Table V), the bond dissociation energy is 138 kJ mol^{-1}. This value may be compared with the lower level estimates of Bouma and Radom[22] (134 kJ mol^{-1}) and Tomoda and Kimura[47] (1.7 eV = 164 kJ mol^{-1}, no zero-point correction used). Tomoda and Kimura[47] have suggested reasons why the value of Ceyer et al.[55] (0.79 eV = 76 kJ mol^{-1}) derived from a molecular-beam–photoionization experiment may not be reliable. The strength of the N–N hemibond leads us to speculate that many systems related to $H_3N{\cdots}NH_3^{\bullet+}$ but without the capacity for isomerization to a hydrogen-bonded species (for example, $(CF_3)_3N{\cdots}N(CF_3)_3^{\bullet+}$), are likely to be stable cations from which solid salts might be prepared. Indeed the crystal structures of two such salts have already been experimentally measured.[2,16]

$H_4O_2^{\bullet+}$ System. The potential surface of the water dimer radical cation is depicted schematically in Figure 4b. The hemibonded ion $H_2O{\cdots}OH_2^{\bullet+}$ (**3**) is metastable, lying 37 kJ mol^{-1} higher in energy than the hydrogen-bonded species $H_2OH{\cdots}OH^{\bullet+}$ (**11**). The barrier to its isomerization is 33 kJ mol^{-1}, which is 9 kJ mol^{-1} less than the corresponding barrier for the ammonia dimer cation discussed above. However, since the unequivocal observation of the hemibonded $H_3N{\cdots}NH_3^{\bullet+}$ ion has recently been reported by Symons et al.[10] (vide supra), we believe that, in an experiment of similar time scale, the hemibonded $H_2O{\cdots}OH_2^{\bullet+}$ may also be sufficiently stable to be detected.

Tomoda and Kimura[50] have pointed out the similar behavior of the neutral ammonia and water dimers upon ionization, noting that, in both cases, a proton transfer takes place spontaneously. The resulting hydrogen bond between a hydronium ion (H_3O^+) and a hydroxyl radical ($OH^{\bullet}$) is approximately linear ($\angle OHO$ = 176°), but with a greater deviation from linearity than that in **10**. Likewise, in the transition structure **17** for isomerization of **3** to **11**, the proton transfer has barely commenced.

The oxygen–oxygen hemibond, despite being more than 2 Å long, is surpassed only by the helium–helium hemibond in strength.

Table VII. Calculated Hydrogen-Bond Lengths[a] (Å) and Dissociation Energies[b] (E_{diss}, kJ mol^{-1}) of the Hydrogen-Bonded Isomers

		H-bond length	$E_{diss}(1)^c$	$E_{diss}(2)^d$
$H_3NH{\cdots}NH_2^{\bullet+}$	**10**	1.744	93	168
$H_2OH{\cdots}OH^{\bullet+}$	**11**	1.524	92	196
$HFH{\cdots}F^{\bullet+}$	**12**	1.435	45	209
$H_3PH{\cdots}PH_2^{\bullet+}$	**13**	2.600	24	98
$H_2SH{\cdots}SH^{\bullet+}$	**14**	2.208	45	61
$HClH{\cdots}Cl^{\bullet+}$	**15**	2.029	39	81

[a] MP2/6-31G*-optimized structures. [b] MP4/6-311G(MC)**//MP2/6-31G* with zero-point correction. [c] Protonation channel: $H_nYH{-}YH_{n-1}^{\bullet+} \rightarrow H_nYH^+ + YH_{n-1}^{\bullet}$. [d] Nonprotonation channel: $H_nYH{-}YH_{n-1}^{\bullet+} \rightarrow H_nY + YH_n^{\bullet+}$. [e] This structure corresponds to a first-order saddle point on the MP2/6-31G* surface (see text).

(55) Ceyer, S. T.; Tiedemann, P. W.; Mahan, B. H.; Lee, Y. T. *J. Chem. Phys.* **1979**, *70*, 14.

However, although the bond dissociation energy at our highest level of theory is 159 kJ mol^{-1}, the Hartree–Fock (6-31G*) dissociation energy is only 96 kJ mol^{-1} (Table IV). Furthermore, at the Hartree–Fock level, the hydrogen-bonded isomer lies 110 kJ mol^{-1} (as compared with out best estimate of 37 kJ mol^{-1}) lower than the hemibonded system. One consequence of this poor description at the single-configuration level is that the hemibonded system is incorrectly found to be a transition structure rather than a minimum on the Hartree–Fock surface.[23d] Satisfactory results are achieved only if the geometries of **11** and of the transition structure **17** linking **3** and **11** are calculated at a correlated level of theory (e.g. MP2/6-31G*), as in the present study.

We believe that, in oxygen–oxygen hemibonded systems for which isomerization to a hydrogen-bonded species is not possible, considerable stability may be anticipated. Indeed, the recent suggestions by Symons et al.[13,14] that the radical cation of dioxane and the species XO–OX$^{\bullet+}$ (where X is, for example, ClO_3) contain such hemibonds seem entirely reasonable in the light of our theoretical results.

$H_2F_2^{\bullet+}$ System. The potential surface of the hydrogen fluoride dimer cation is depicted schematically in Figure 4c. The hemibonded ion HF···FH$^{\bullet+}$ (**4**) is metastable, lying 51 kJ mol^{-1} higher in energy than the isomeric hydrogen-bonded species HFH···F$^{\bullet+}$ (**12**). However, the barrier to its isomerization is 48 kJ mol^{-1}. Consequently, although HF···FH$^{\bullet+}$ is thermodynamically less stable with respect to its hydrogen-bonded isomer than either $H_3N{\cdots}NH_3^{\bullet+}$ or $H_2O{\cdots}OH_2^{\bullet+}$, it is actually kinetically more stable than either of them. Additionally, the dissociation energy of its three-electron hemibond is comparable to that of the strong oxygen–oxygen hemibond discussed above.

The formation of the hydrogen-bonded HFH···F$^{\bullet+}$ dimer (**12**) from HF and HF$^{\bullet+}$ involves a spontaneous proton transfer (as is also found for the ammonia and water dimer cations), and the resulting structure **12** may be viewed as a complex of H_2F^+ and F$^\bullet$ with a binding energy of 45 kJ mol^{-1}. This hydrogen-bond strength is significantly less than those of the ammonia or water dimer cations (Table VII).

Despite the considerable dissociation energy of the F–F hemibond (158 kJ mol^{-1}) at our highest level of theory, it is predicted to be much weaker at the Hartree–Fock level (Table IV). Indeed, as was the case for the water dimer cation, the hemibonded isomer is incorrectly predicted to be a transition structure rather than a minimum on the Hartree–Fock potential surface.[23d] Again, a satisfactory description of the potential energy surface is achieved only through geometry optimizations at correlated levels of theory.

We note in passing that although the hemibonded and hydrogen-bonded forms of $H_2F_2^{\bullet+}$ both possess a plane of symmetry, their ground-state wave functions are of $^2A'$ and $^2A''$ symmetry respectively (in the C_s point group), and hence the transition structure **18** linking them has C_1 symmetry.

The apparent strength of the fluorine–fluorine hemibond is sufficiently large that we believe that molecules that contain such bonding, but in which rearrangement to a hydrogen-bonded isomer is precluded, should be expected to exhibit substantial stability.

$P_2H_6^{\bullet+}$ System. The potential surface of the phosphine dimer cation is depicted schematically in Figure 4d. In marked contrast to the first-row systems, the hemibonded and hydrogen-bonded isomers of $P_2H_6^{\bullet+}$ are very close in energy, the hemi-bonded species being preferred by just 5 kJ mol^{-1} at our highest level of theory.

The isomers **6** and **13** are separated by a barrier of 52 kJ mol^{-1}, but this is substantially larger than the dissociation energy (24 kJ mol^{-1} via the protonation channel) of the hydrogen-bonded species. Although the well corresponding to the hydrogen-bonded ion $H_3PH{\cdots}PH_2$ (**13**) would support a number of bound vibrational states, its shallowness should render the experimental observation of this isomer, *under conditions of thermal equilibrium*, rather difficult at normal temperatures. Nonethless, in a collision-free environment, or at very low temperatures, the species could be sufficiently long lived to be experimentally observable.

The hemibonded system **6** is considerably more kinetically stable. The channel leading to isomerization is the lowest energy decomposition pathway for $H_3P{\cdots}PH_3^+$ and the isomerization barrier is 10 kJ mol^{-1} larger than that for $H_3N{\cdots}NH_3^+$; thus, in light of the positive result of the Symons ESR experiment[10] on $H_3N{\cdots}NH_3^{\bullet+}$, it seems that $H_3P{\cdots}PH_3^{\bullet+}$ is a strong candidate for experimental observation. Indeed, substituted derivatives of the prototypical $H_3P{\cdots}PH_3^{\bullet+}$ were first observed many years ago[15] and are now very well characterized experimentally.[12]

We find that the minimum-energy structure for $H_3P{\cdots}PH_3^{\bullet+}$ (**6**) has C_{2h} symmetry, and it is interesting to consider whether an ESR experiment should detect a single set of six equivalent protons (the result of the time averaging of all possible C_{2h} structures) or two sets of four and two equivalent protons, respectively (which would be expected if a single C_{2h} species were observed). The D_{3d} structure of $H_3P{\cdots}PH_3^{\bullet+}$ is a second-order saddle point on the potential surface (when polarization functions are included in the basis set) but lies only about 3 kJ mol^{-1} (UHF/6-31G*) higher in energy than the C_{2h} minimum. Thus (except perhaps at liquid helium temperatures), the exchange of the formally nonequivalent hydrogen atoms in the C_{2h} structure will be rapid on the ESR time scale, and we anticipate that the ESR spectrum (at, for example, 77 K) should reveal six equivalent protons.

The intrinsic strength of the P–P hemibond (103 kJ mol^{-1}) is the second-lowest of the nine investigated. It is a significant bond nonetheless, and larger systems that contain such bonding and in which isomerization to a hydrogen-bonded isomer is not possible are likely to be fairly stable.

$H_4S_2^{\bullet+}$ System. The potential surface of the hydrogen sulfide dimer cation is depicted schematically in Figure 4e. We find that, unlike the first-row systems, the hemibonded $H_2S{\cdots}SH_2^{\bullet+}$ (**7**) is *lower* in energy than its hydrogen-bonded isomer $H_2SH{\cdots}SH^{\bullet+}$ (**14**) by 50 kJ mol^{-1}. Moreover, although the transition structure **20** for the interconversion of **7** and **14** could be found at the HF/6-31G* level, a search for it at the MP2/6-31G* level was unsuccessful. A subsequent calculation revealed that, at the correlated level, the hydrogen-bonded species collapses spontaneously to the hemibonded isomer when the C_s symmetry constraint is relaxed. It appears, therefore, that the *only* minimum on the potential surface of $H_4S_2^{\bullet+}$ is the three-electron hemibonded $H_2S{\cdots}SH_2^{\bullet+}$ (**7**). This result contrasts with the findings at the Hartree–Fock level[31,53] and reconfirms the importance of *correlated* geometry optimizations of these systems.

The energies required for dissociation of $H_2S{\cdots}SH_2^{\bullet+}$ into $H_2S + H_2S^{\bullet+}$ or $H_3S^+ + SH^\bullet$ are calculated to be 111 and 95 kJ mol^{-1}, respectively. In a recent photoionization study of $(H_2S)_2^{\bullet+}$, Prest et al.[56] estimated the bond dissociation energy of $(H_2S)_2^{\bullet+}$ to be 0.92 ± 0.04 eV (88 ± 4 kJ mol^{-1}), which is in good agreement with the value we calculate for the protonation channel. They do not propose a structure for $(H_2S)_2^{\bullet+}$ but its dissociation energy suggests very strongly that they were observing the hemibonded species.

Asmus et al.[6-9] have unambiguously identified a variety of cations $R_2S{\cdots}SR_2^{\bullet+}$ (which are substituted forms of the prototype $H_2S{\cdots}SH_2^{\bullet+}$) in solution and have measured their optical absorption spectra using pulse radiolysis techniques. They propose that the transition with λ_{max} = 370 nm in the spectrum of $H_2S{\cdots}SH_2^{\bullet+}$ arises from the $\sigma \rightarrow \sigma^*$ transition in the three-electron bond, and Clark[23a] found that the theoretical value (estimated as the difference betweeen the appropriate orbital energies) using the 4-31G basis set was 3.25 eV (380 nm), which is in good agreement with Asmus' value. Unfortunately, we find that the agreement becomes less satisfactory when a better basis set is used (2.76 eV (320 nm), using 6-31G*), but this probably reflects the quantitative inadequacy of Koopmans' theorem as much as anything else.

While the existence of $R_2S{\cdots}SR_2^{\bullet+}$ species in solution has been established beyond any doubt, until very recently such ions had not been observed in the gas phase. However, Drewello et al. have now successfully prepared and studied the free hemibonded di-

(56) Prest, H. F.; Tzeng, W.-B.; Brom, J. M.; Ng, C. Y. *J. Am. Chem. Soc.* **1983**, *105*, 7531.

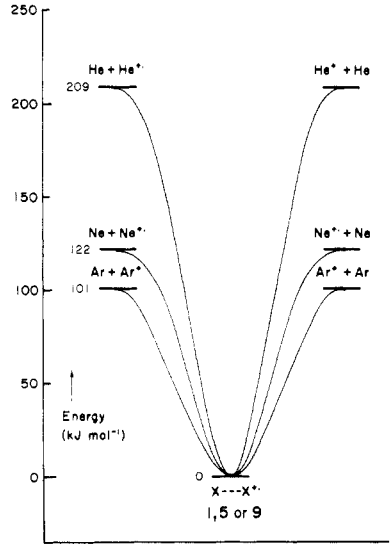

Figure 5. Schematic potential energy curves showing dissociative processes in the inert-gas ion dimers He···He$^{\bullet+}$ (**1**), Ne···Ne$^{\bullet+}$ (**5**), and Ar···Ar$^{\bullet+}$ (**9**).

isopropyl sulfide dimer radical cation using both Fourier transform ion cyclotron resonance and tandem mass spectrometry techniques.[57] On the basis of our observations regarding substituent effects on three-electron hemibonds (vide infra), we expect that the diisopropyl sulfide dimer radical cation should be more weakly bound than $H_2S{\cdots}SH_2^{\bullet+}$.

It is truly remarkable that the hemibonded $H_2S{\cdots}SH_2^{\bullet+}$ ion (**7**) is such a stable species. Despite the fact that the S–S bond length in this molecule is more than 2.8 Å (that is, 1 Å longer than that in the S_2 molecule and the longest of all the three-electron bonds studied in this paper), we find that 111 kJ mol^{-1} is required to break this S–S bond and, in addition, that the hemibonded dimer **7** is the global minimum on the $H_4S_2^{\bullet+}$ surface.

$H_2Cl_2^{\bullet+}$ System. The potential surface of the hydrogen chloride dimer cation is depicted schematically in Figure 4f. Although the hydrogen-bonded HClH···Cl$^{\bullet+}$ ion (**15**) is lower in energy than the hemibonded system **8** at the uncorrelated HF/6-31G* level (Table IV), correlation stabilizes **8** relative to **15**, and, at our highest level of theory, the hemibonded species is the global minimum on the surface. The hydrogen-bonded ion is 34 kJ mol^{-1} higher in energy, and the transition structure for their interconversion (**21**) is a further 34 kJ mol^{-1} higher again.

The hydrogen-bonded HClH···Cl$^{\bullet+}$ ion (**15**) can isomerize to HCl···ClH$^{\bullet+}$ (**8**) or dissociate via the protonation channel, and in neither case is the barrier more than 40 kJ mol^{-1}. For this reason, the existence of the hydrogen-bonded isomer is unlikely to be more than fleeting unless either low temperatures are used or the molecules are prevented from reaching thermal equilibrium within the time scale of the experiment.

On the other hand, the hemibonded HCl···ClH$^{\bullet+}$ ion (**8**) seems likely to be a comparatively stable species. Although it can rearrange to $H_2Cl{\cdots}Cl^{\bullet+}$ (**15**), this isomerization is both thermodynamically and kinetically unfavorable. The dissociation pathway leading to $H_2Cl^+ + Cl^\bullet$ is inhibited by a barrier of 73 kJ mol^{-1}, while that leading to the direct fission of the hemibond requires 115 kJ mol^{-1}. Symons et al.[11] have recently measured and analyzed the ESR spectrum of a radical cation, which they consider to be the Cl–Cl hemibonded dimer cation of trichlorofluoromethane. Our results for HCl···ClH$^{\bullet+}$ taken together with our substituent effect conclusions (vide infra) suggest that $(Cl_2FCCl)_2^{\bullet+}$ should be a particularly strongly bound species, thus supporting Symons' assignment.

The Cl–Cl hemibond is the strongest of all the second-row hemibonds (Table V). We conclude, therefore, that both the prototypical HCl···ClH$^{\bullet+}$ ion and its higher homologues (such as Symon's hemibonded dimer cation of $CFCl_3$) should be rather stable systems and warrant experimental investigation.

(57) Drewello, T.; Lebrilla, C. B.; Schwarz, H.; de Koning, L. J.; Fokkens, R. H.; Nibbering, N. M. M.; Anklam, E.; Asmus, K.-D. *J. Chem. Soc., Chem. Commun.* **1987**, 1381.

Table VIII. Calculated Effects of Substituents on the O–O Bond Length (Å) and Dissociation Energy (D_e, kJ mol^{-1}) of Hemibonded $H_2O{\cdots}OH_2^{\bullet+}$ [a]

X	$D_e(X{\cdots}X^{\bullet+})$	r_{O-O}	$E_{HOMO}(X)$ [b]
H_2O	139	1.909	−0.477
$(CH_3)_2O$ [c]	43	1.962	−0.410
$(CH_2F)OH$ [d]	104	1.900	−0.458

[a] UHF/3-21G. [b] E_{HOMO} values in hartrees. [c] Fully optimized, C_{2h} symmetry. [d] Individual fluoromethanol units constrained to have C_s symmetry; the hemibonded dimer cation constrained to have C_i symmetry.

$He_2^{\bullet+}$, $Ne_2^{\bullet+}$, and $Ar_2^{\bullet+}$ Systems. The potential curves of the inert-gas dimer cations are depicted schematically in Figure 5. In all cases, the hemibonded dimer is the only, and hence the global, minimum on the potential surface and dissociates, without reverse activation energy, to give an inert-gas atom and its cation. The trend of decreasing stability as the atom involved becomes less electronegative (He > Ne > Ar) is clear and is anticipated from the Hückel model, which we derived above.

As was noted earlier, the He···He$^{\bullet+}$ system has been well studied in the past, both experimentally and theoretically. From the results of a large CI calculation, Liu[33] has calculated that the dissociation energy D_e of $He_2^{\bullet+}$ is at least 2.454 eV (237 kJ mol^{-1}) and is probably 2.469 ± 0.006 eV (238.2 ± 0.6 kJ mol^{-1}). This value does not include a correction for zero-point energy, which Huber and Herzberg[44] estimate from differential scattering experiments and which they use to estimate that D_0 = 2.365 eV (228 kJ mol^{-1}). In comparison, our theoretical estimate of D_0 is 209 kJ mol^{-1}, indicating that our standard level of theory (MP4/6-311G(MC)**//MP2/6-31G*, with zero-point correction) recovers about 92% of the $He_2^{\bullet+}$ three-electron hemibond energy. It is interesting to note that, if we assume that the binding contributions from a set of d functions on He and from a second set of p functions are additive, we can use the results in Table I to estimate D_e at the MP4/6-311G(MC)(,2pd) level to be 231 kJ mol^{-1}, which is very close the Huber and Herzberg result.

The experimental value of D_e(Ne···Ne$^{\bullet+}$) = 1.30 eV (125 kJ mol^{-1}), given by Huber and Herzberg,[44] coincides with the value of 125 kJ mol^{-1} obtained at our standard level of theory (Table IV). However, it appears from Table I that the true value may be a little larger than these. In particular, although f functions seem to be unimportant, the addition of a second set of d functions to the neon basis set leads to an increase of 10 kJ mol^{-1} in the hemibond dissociation energy.

The Ar···Ar$^{\bullet+}$ dimer also appears to be well-behaved. We calculate D_0 = 101 kJ mol^{-1} (Table V), which is in good agreement with the experimental value, again given by Huber and Herzberg,[44] of ≥1.049 eV (101 kJ mol^{-1}), but, as was pointed out for the Ne···Ne$^{\bullet+}$ ion above, it seems likely that further improvement in the polarization part of the basis set will lead to a significantly greater dissociation energy. Our best estimate (Table I) corresponds to D_e = 117 kJ mol^{-1} (or D_0 = 118 kJ mol^{-1}).

From the favorable comparisons between the experimental values and our theoretical hemibond dissociation energies for the well-studied inert-gas dimer cations, we feel justified in believing that our results for the *other* hemibonded systems considered in this paper are probably reliable.

Substituent Effects in the Hemibonded Water Dimer Cation. In a recent paper, Asmus et al.[8] found that the effect of substituents on the strengths of S···S hemibonds can be very large. They have used the wavelength λ_{max} arising from the $\sigma \rightarrow \sigma^*$ optical transition as an inverse measure of the bond strength and have measured λ_{max} for nine $R_2S{\cdots}SR_2^{\bullet+}$ species, R=H, CH_3, C_2H_5, C_3H_7 (two isomers), and C_4H_9 (four isomers). They find an excellent correlation between the energy of the optical transition and Taft's[58] inductive σ^* parameter for R. They explain the

(58) Taft, R. *J. Am. Chem. Soc.* **1953**, *75*, 4231.

hemibond weakening as arrising from electron induction into the antibonding σ^* orbital.

In Table VIII we compare the O–O bond lengths and dissociation energies in the dimer cations of H_2O, $(CH_3)_2O$, and $(FCH_2)OH$. These were calculated at the simple UHF/3-21G level, and the results should be viewed in a comparative rather than an absolute sense. The effect of the electron-donating methyl groups on the hemibond strength is marked, reducing it in the dimethyl ether dimer cation to less than one-third of its value in the water dimer cation. Methyl substitution also changes the O–O hemibond length, but this is a much smaller effect (0.05 Å). The fluorine atom exerts an opposing electron-withdrawing influence, however, and almost entirely counterbalances the bond-weakening effect of the methylene groups in the dimer cation of fluoromethanol. In fact, we find that the O–O bond in this system is marginally shorter than that in the hemibonded water dimer cation.

Our qualitative Hückel model for the three-electron hemibond in $X–X^{\bullet+}$ predicts that the strength of the bond should vary in proportion to the Hückel α parameter, which we may replace, at least for comparison purposes, by the HOMO energy in X. The correlation between $E_{HOMO}(X)$ and $D_e(X\cdots X^{\bullet+})$ (Table VIII) is therefore pleasing.

It is apparent from these results that, as Asmus has found,[8] the substituents close to a three-electron hemibond have a marked effect on the strength of the bond. Extrapolation from the results in Table VIII leads, for example, to the prediction that a large increase in stability should be found experimentally along the series of oxygen–oxygen hemibonded dimer cations from that of methanol to that of trifluoromethanol.

Concluding Remarks

Several important points emerge from this theoretical study:

(1) The dimer cations of first- and second-row hydrides can generally exist both as hemibonded and hydrogen-bonded isomers. The hydrogen-bonded isomers are favored for all the first-row systems; the two isomers have comparable energies in the case of $P_2H_6^{\bullet+}$, while for the other second-row systems the hemibonded isomers are preferred.

(2) In all cases, direct fission of the hydrogen bond rather than of the hemibond represents the lowest energy dissociation pathway.

(3) Three-electron hemibonds are remarkably strong, with calculated bond dissociation energies greater than 100 kJ mol^{-1} in all cases. They are strengthened further by adjacent electron-withdrawing substituents. If rearrangement to hydrogen-bonded species (leading to the lower energy dissociation process) is precluded by appropriate substitution, systems containing any of the hemibonds examined in this paper should be readily observable.

(4) The hydrogen-bonded species are best described as complexes between protonated and deprotonated monomer units, the proton transfer occuring spontaneously during dimerization.

(5) The barriers to rearrangement and dissociation are sufficiently large that, under appropriate conditions, both the hemibonded and hydrogen-bonded isomers of all systems except $H_4S_2^{\bullet+}$ should be individually observable. For $H_4S_2^{\bullet+}$, the hydrogen-bonded structure is predicted to rearrange with little or no barrier to the hemibonded isomer.

(6) High levels of ab initio theory are required in order to obtain reliable descriptions of the potential energy surfaces. In three cases, geometry optimization at correlated levels of theory leads to even *qualitative* differences in the description of the surfaces compared with the Hartree–Fock results.

Acknowledgment. We thank Tim Clark, Joseph Dinnocenzo, Richard Glass, and Helmut Schwarz for copies of their papers prior to publication and Willem Bouma, Dieter Asmus, and Roger Alder for helpful discussions and correspondence.

Registry No. He_2^+, 12184-99-5; $(NH_3)_2^+$, 93943-00-1; $(H_2O)_2^+$, 64236-54-0; $(HF)_2^+$, 112896-81-8; Ne_2^+, 12185-06-7; $(PH_3)_2^+$, 87147-40-8; $(H_2S)_2^+$, 77386-59-5; $(HCl)_2^+$, 87141-21-7; Ar_2^+, 17596-58-6; He, 7440-59-7; Ne, 7440-01-9; Ar, 7440-37-1; HF, 7664-39-3; NH_3, 7664-41-7; PH_3, 7803-51-2; H_2S, 7783-06-4; HCl, 7647-01-0; H_2O, 7732-18-5; He^+, 14234-48-1; Ne^+, 14782-23-1; Ar^+, 14791-69-6; HF^+, 12258-94-5; NH_3^+, 19496-55-0; PH_3^+, 29724-05-8; H_2S^+, 26453-60-1; HCl^+, 12258-94-5; H_2O^+, 56583-62-1.